Applied Acoustics 249 (2026) 111308

Contents lists available at ScienceDirect

Applied Acoustics

journal homepage: www.elsevier.com/locate/apacoust

Acoustic and mechanical properties of bio-based mycelium materials from oyster mushroom species: comparative analysis of *Pleurotus ostreatus* and *Pleurotus eous*

Tanyaporn Damthip [a], Nur-asrin Hama [a], Sakchai Khongnakhon [b], Benjawan Yanwisetpakdee [c], Polphat Ruamcharoen [d,e], Purintorn Chanlert [a,e,*]

[a] *Program of Physics, Faculty of Science and Technology, Songkhla Rajabhat University, Mueang, Songkhla 90000 Thailand*
[b] *Program of Innovative Agriculture for Sustainability, Faculty of Science and Technology, Songkhla Rajabhat University, Mueang, Songkhla 90000 Thailand*
[c] *Program of Biology, Faculty of Science and Technology, Songkhla Rajabhat University, Mueang, Songkhla 90000 Thailand*
[d] *Program of Rubber and Polymer Technology, Faculty of Science and Technology, Songkhla Rajabhat University, Mueang, Songkhla 90000 Thailand*
[e] *Research Unit in Applied Physics and Advanced Materials (APAM), Faculty of Science and Technology, Songkhla Rajabhat University, Mueang, Songkhla 90000 Thailand*

ARTICLE INFO

Keywords:
Pleurotus ostreatus
Pleurotus eous
Bio-based materials
Mycelium-based composites
Sound absorption

ABSTRACT

This research investigates the acoustic and mechanical trade-offs of mycelium-based composites (MBCs) derived from two fungal species: *Pleurotus ostreatus* (*P. ostreatus*) and *Pleurotus eous* (*P. eous*). Cultivated on a sawdust substrate with varying starch contents (3–9%) and molded into two thicknesses (20 and 40 mm), the composites were evaluated for their sound absorption coefficient (SAC) and compressive strength. Results indicate that MBCs made from *P. eous* (EOU) exhibit noise reduction coefficient (NRC) values of approximately 0.42–0.52, whereas those made from *P. ostreatus* (OST) show lower NRC values of approximately 0.27–0.34, depending on thickness. Conversely, MBCs made from *P. ostreatus* (OST) developed a denser hyphal structure (16.67 μm hyphal diameter compared to 13.8 μm for EOU), resulting in higher compressive yield strengths (19.6–24.3 kPa) but lower NRCs due to surface densification and increased impedance. ANOVA indicates species-specific design trends, with starch content exerting a measurable influence on the NRC of OST samples, while specimen thickness plays a more dominant role in governing the NRC and the average sound absorption at low and high frequency ranges of EOU samples. Crucially, starch modification for acoustic tuning did not compromise the mechanical integrity of either species. These findings suggest that while EOU is ideal for high-performance sound absorbers, OST offers a balanced solution for semi-structural, non-load-bearing acoustic applications, providing a framework for the species-driven design of sustainable building materials.

1. Introduction

The construction industry drives global development but is a major contributor to climate change, with conventional materials like concrete generating ~ 5% of global CO_2 emissions through processes such as ordinary portland cement (OPC) production [1]. In response, researchers have explored sustainable, bio-based alternatives that offer lower environmental impact and improved energy efficiency in the built environment [2]. These materials aim to enhance building performance while reducing pollution and resource consumption, aligning with global efforts to develop low-carbon, resilient, and circular building systems [3,4].

Beyond environmental performance, buildings must also address acoustic comfort, which is essential for occupant well-being. Consequently, natural porous materials have been widely investigated as sound absorbers and acoustic insulators [5]. Such materials are commonly classified as cellular, granular, or fibrous absorbers, depending on their internal structure and sound attenuation mechanisms [6]. Cellular absorbers, including bio-based foams [7,8] and aerogels [9], dissipate sound through interconnected pore networks. Granular absorbers, such as recycled crumb rubber [10], fruit stone [11], and termite mound soil [12] rely on particle interactions to scatter and absorb acoustic energy. Fibrous absorbers—including sugarcane bagasse [13], kenaf [14], water hyacinth [15], nipa palm [16] and

* Corresponding author at: Faculty of Science and Technology, Songkhla Rajabhat University, Mueang, Songkhla 90000 Thailand
E-mail address: purintorn.ch@skru.ac.th (P. Chanlert).

https://doi.org/10.1016/j.apacoust.2026.111308
Received 30 October 2025; Received in revised form 14 February 2026; Accepted 12 March 2026
Available online 21 March 2026

palmyra palm [17], —utilize interwoven fiber structures to enhance broadband sound absorption. In addition, tropical wood materials have attracted increasing interest as natural sound absorbers. Species such as Cajuput (*M. cajuputi*), Mangium (*A. mangium*), and Mango (*M. indica*) have demonstrated promising acoustic performance owing to their inherent porosity, wide availability, and suitability for enhancement through simple, eco-friendly modifications [18]. These materials provide a sustainable alternative to conventional acoustic treatments, contributing to acoustically optimized buildings [19,20].

Within this broader context, mycelium—the vegetative network of fungi—has emerged as a particularly promising bio-based material for applications ranging from packaging to construction [21,22]. Growing concern over the ecological footprint of traditional construction materials has driven increasing interest in mycelium-based composites (MBCs) as renewable, biodegradable, and low-impact alternatives [23,24]. The intrinsic microstructure of mycelium, characterized by interconnected fibrous networks, contributes to its mechanical integrity and functional versatility, making it an attractive candidate for sustainable construction materials [25]. Among various fungal genera, *Pleurotus* has received considerable attention due to its ability to form dense and resilient mycelial mats suitable for biofabrication [26]. While prior studies have investigated thermal insulation, fire resistance, and biodegradability of MBCs [27,28], their acoustic behavior and mechanical performance—particularly in comparative, species-specific contexts—remain insufficiently explored [29,30].

Among *Pleurotus* species, *Pleurotus ostreatus* (grey oyster mushroom, *P. ostreatus*) is known for its rapid mycelial growth and ability to form dense fibrous networks [31]. Similarly, *Pleurotus eous* (*P. eous*), commonly referred to as the pink oyster mushroom or oyster mushroom-Bhutan, has gained recognition as an edible species. This species has recently become more popular due to its ability to grow on diversified substrates and its tolerance to a wide range of temperatures, making it suitable for cultivation in various climates. Additionally, some *Pleurotus* species are known for its high yield potential, which are attractive traits for commercial mushroom production [32,33]. Beyond their culinary value, the very traits that make these *Pleurotus* species desirable for cultivation—rapid, dense growth and substrate versatility—also make them ideal candidates for biofabrication [34]. Utilizing mycelium as a natural, self-growing binder enables the valorization of abundant agricultural waste into functional, low-carbon, and fully biodegradable composites, addressing the environmental burden of conventional construction materials [35,36]. Despite this promise, the acoustic performance, noise reduction coefficient (NRC), frequency-dependent sound absorption behavior, and key mechanical properties of *Pleurotus*-based composites have not yet been systematically compared. In particular, compressive yield strength and elastic modulus must be evaluated to assess their suitability for lightweight, non-load-bearing construction applications [37].

Accordingly, this study presents a controlled comparison of the acoustic and mechanical properties of MBCs derived from *Pleurotus ostreatus* (OST) and *Pleurotus eous* (EOU). Using a full factorial design, the effects of fungal species, starch content, and specimen thickness on frequency-dependent sound absorption, NRC, and compressive response are systematically evaluated. Microstructural features observed by optical and scanning electron microscopy are analyzed to explain species-dependent absorption behavior. The MBCs investigated in this study are intended for non-structural interior acoustic applications, such as sound-absorbing panels, where lightweight construction, sustainability, and sound absorption performance are prioritized, rather than sound insulation or load-bearing structural uses. The results provide acoustically relevant design insight for the development of bio-based porous absorbers.

2. Materials and methods

2.1. Sample preparation

2.1.1. Spawn cultivation

The MBCs were prepared using *P. ostreatus* (OST) and *P. eous* (EOU) as the fungal strains. Spawn cultures were developed by inoculating sterilized potato dextrose agar (PDA) plates with the respective mushroom strains. The plates were incubated at ambient conditions for 10–15 days to ensure complete colonization of the agar medium by the fungal mycelium. Once the plates were fully colonized, the cultures were ready for inoculation into the prepared substrates.

2.1.2. Substrate formulation

Three substrate formulations were developed using sawdust as the primary base, supplemented with rice flour, rice bran, gypsum, yeast extract, molasses, and distilled water. The specific proportions for each formulation are detailed in Table 1. To prepare the substrates, the dry components (sawdust, rice bran, gypsum, and yeast extract) were blended first, while the molasses and rice flour were dissolved in deionized water prior to being thoroughly mixed with the dry base.

2.1.3. Sterilization and inoculation

The resulting mixture was packed into heat-resistant plastic bags and sealed securely. The substrate bags, along with cylindrical stainless-steel molds for shaping the composites, were sterilized in an autoclave at standard sterilization conditions to eliminate microbial contamination. Following sterilization, the inoculation process was carried out in a laminar airflow cabinet to maintain aseptic conditions. Fully colonized PDA plates of *Pleurotus* strains were inspected for viability, and mycelial plugs were extracted 1 cm from the edges using a sterilized cork borer. Six mycelial plugs were introduced into each substrate bag, ensuring even distribution of fungal inoculum throughout the substrate. The bags were gently shaken to facilitate uniform mixing of the inoculum with the substrate and then sealed with rubber bands.

2.1.4. Incubation and supplementation

The inoculated substrate bags were incubated in a dark, temperature-controlled room at an average temperature of

Table 1
Percentage composition of substrate formulations for fungal cultivation.

Component	Formulation 1 (%)	Formulation 2 (%)	Formulation 3 (%)
Sawdust	50.0	48.3	46.7
Rice flour	3.0	5.8	8.4
Rice bran	10.0	10.0	10.0
Gypsum	2.0	2.0	2.0
Yeast extract	0.5	0.5	0.5
Molasses	2.0	2.0	2.0
Deionized water	32.5	31.4	30.4
Sample name	OST-1S, OST-1L, EOU-1S, EOU-1L	OST-2S, OST-2L, EOU-2S, EOU-2L	OST-3S, OST-3L, EOU-3S, EOU-3L

*Note: In *Sample name* row, OST and EOU denote *P. ostreatus* and *P. eous*, respectively. The numerals 1, 2, and 3 correspond to substrate formulations 1, 2, and 3. The letters S and L indicate sample thickness, where S represents 20 mm and L represents 40 mm.

approximately 25°C for 20 days. During this period, the mycelium grew and completely colonized the substrate. After the initial incubation, additional rice flour was introduced into each bag to enhance binding properties. The quantities added were 3.0 g, 5.8 g, and 8.4 g for Formulations 1, 2, and 3, respectively. The rice flour was evenly mixed into the substrate to ensure homogeneity.

2.1.5. Molding and secondary incubation

To prepare the samples, substrates were compacted into cylindrical molds with a diameter of 28.6 mm and two distinct thicknesses (20 mm and 40 mm). As detailed in Table 1, samples were categorized by fungal species—*P. ostreatus* (OST) and *P. eous* (EOU)—substrate formulation (1, 2, or 3), and thickness (S for 20 mm; L for 40 mm). The "S" samples were prepared by filling 20 mm molds with 5 g of substrate, while the "L" samples utilized 40 mm molds filled with 10 g of substrate. Following molding, all samples underwent a secondary incubation for five days in a ventilated enclosure, allowing the mycelium to bind the substrate into a cohesive, solid structure.

2.1.6. Drying and conditioning

After incubation, the formed MBC samples were carefully removed from the molds and dried in a hot-air oven at 70°C for 3 h. The dried composites were then conditioned in a humidity-controlled cabinet maintained at 25°C and 40% relative humidity for at least 5 days. This step ensured the stabilization of the samples before further characterization and testing for density and sound absorption properties as illustrated in Fig. 1 [38].

2.2. Surface morphology

Surface morphology of the MBCs was examined using optical microscopy (OM) and scanning electron microscopy (SEM). OM was first employed to observe the macroscopic surface features and overall texture of the specimens. Representative images were captured to assess surface roughness, visible porosity, and the distribution of mycelial networks on the composite surface. Microstructural characterization was subsequently conducted using a scanning electron microscope (Hitachi SU3900, Hitachi High-Tech, Tokyo, Japan). Prior to SEM observation, samples were cut to appropriate size and sputter-coated with a thin conductive layer to minimize charging effects. SEM imaging was performed to investigate the hyphal network morphology, pore structure, and connectivity at higher magnifications. Hyphal diameters were estimated from SEM micrographs by averaging multiple fibers taken from representative regions in the SEM image.

2.3. Sound absorption property

To determine the sound absorption coefficient (SAC) spectra of the MBC samples, an in-house cylindrical impedance tube was employed [15–17], utilizing the two-microphone method for precision. The impedance tube, crafted from stainless steel, had an internal diameter of 28.6 mm, to minimize noise interference and ensure reliable measurements. The design adhered to international standards ASTM E1050 [39] and ISO 10534–2 [40], which outline methods for determining acoustic properties of materials using the transfer function technique. This setup allowed for accurate analysis of the interaction between incident and reflected sound waves within the tube. The measurement system included two high-precision laboratory-grade microphones (GRAS 46BD-FV, GRAS Sound & Vibration, Denmark) positioned and sealed securely within the tube. The hermetic placement of the microphones ensured that external noise and air leaks did not compromise the measurements. A broadband noise signal, generated by a full-range speaker located at one end of the tube, provided the sound waves needed for testing. The samples were mounted in a holder at the opposite end of the tube, backed by a rigid plate made from stainless steel to eliminate vibrations or unwanted movement during measurements. The acoustic

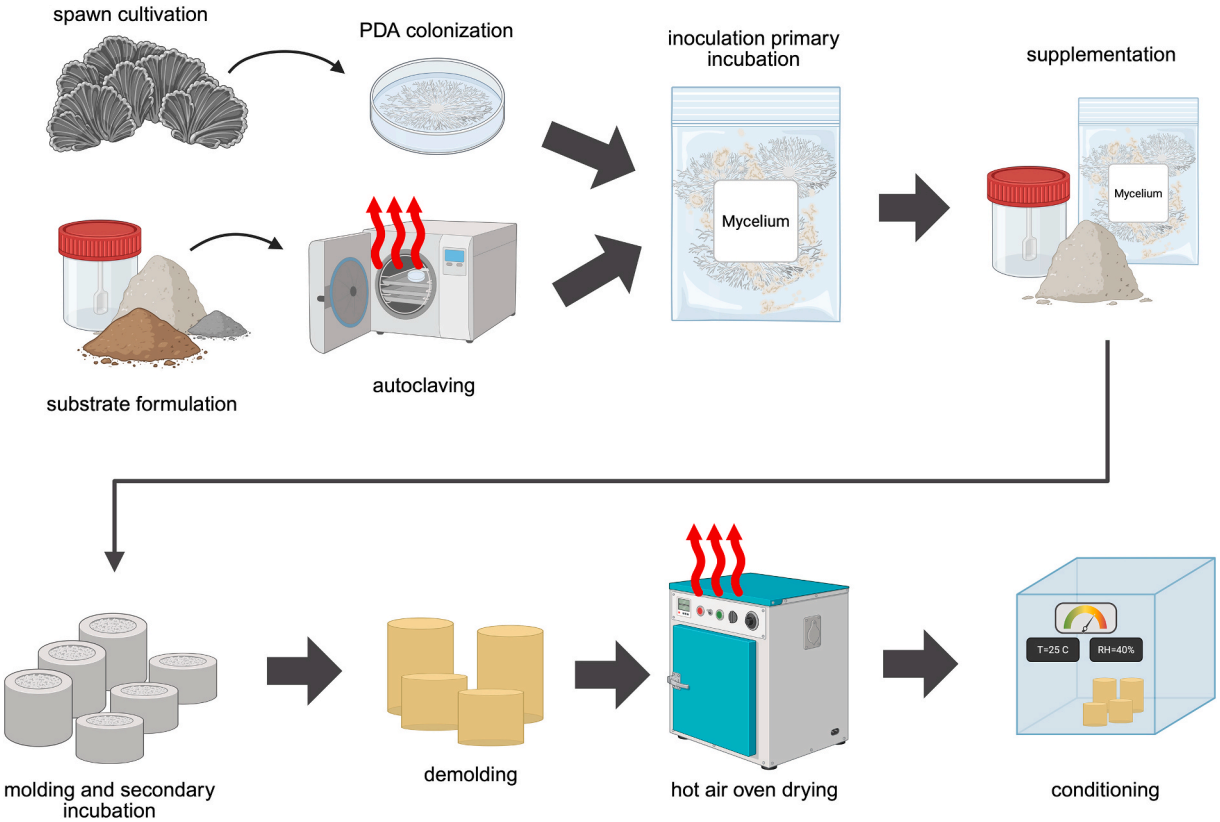

Fig. 1. Schematic representation of the preparation procedure of MBCs, including spawn cultivation, substrate mixing, inoculation, molding, and drying stages. [38].

signals were captured by the microphones and processed through a high-resolution data acquisition device (NI-9230, National Instruments, USA) using Python. The transfer function method was employed to compute the SAC as follows:

$$\mathrm{SAC}(f) = 1 - \left| \frac{H_{12}(f) - e^{-jks}}{e^{jks} - H_{12}(f)} e^{2jkx_1} \right|^2 \quad (1)$$

where H_{12} is the transfer function between the sound signals measured by microphone 1 (mic-1) and microphone 2 (mic-2), k is the complex wave number of the sound wave in the air, and s and x_1 are the distances between two microphones (mic-1 and mic-2) and between the sample surface and the first microphone (mic-1), respectively. Average values from the three replicates for each formulation were calculated. A schematic diagram of the two-microphone impedance tube system is shown in Fig. 2(a), together with a photograph of the experimental setup in Fig. 2(b) and an image of a cylindrical specimen mounted in the sample holder in Fig. 2(c).

2.4. Mechanical property

The mechanical properties of the MBCs, specifically yield strength and compressive modulus, were evaluated using a universal testing machine (NRI-TS500-30B, Narin Instrument, Thailand). These cylindrical OST and EOU were prepared following the sample preparation protocol described earlier. The machine was configured with a crosshead speed of 1.0 mm/min, ensuring uniform application of compressive force across all samples. During the compression test, the samples were subjected to a steadily increasing load, and yield strength was determined using the 0.2% offset method from the stress–strain curve [41]. This method involves drawing a parallel line to the initial linear elastic portion of the stress–strain curve, offset by 0.2% strain along the x-axis. The intersection of this offset line with the stress–strain curve defines the yield strength, representing the stress at which the material exhibits significant plastic deformation. The compressive modulus, representing the material's stiffness, was calculated from the stress–-strain relationship in the linear elastic region of the curve. Average values from the three replicates for each formulation were calculated.

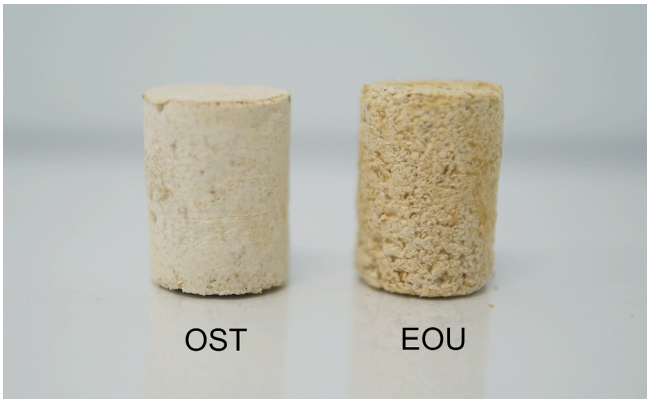

Fig. 3. Photograph of cylindrical MBCs produced from *P. ostreatus* (OST) and *P. eous* (EOU).

3. Results and Discussion

3.1. Sample characteristics

From Fig. 3, OST exhibited a smoother and more uniform surface appearance compared to samples of EOU, which displayed a prominent porous texture. This visual difference highlights the unique growth patterns and structural characteristics of the mycelium from each species, which contribute significantly to their physical and acoustic properties. Dimensional shrinkage is observed after thermal drying of the mycelium composite samples. Although the freshly demolded specimens initially match the mold dimensions (28.6 mm diameter, with thicknesses of 40 mm for large samples and 20 mm for small samples), noticeable shrinkage occurs after drying in an air-circulating oven at 70°C. For OST samples, diameter shrinkage reaches 3.2% (OST-L) and 5.1% (OST-S), while thickness shrinkage reaches 11.9% (OST-L) and 9.8% (OST-S). In contrast, EOU exhibits greater radial shrinkage (6.4% and 6.5% for EOU-L and EOU-S, respectively) but lower axial shrinkage, at 5.9% (EOU-L) and 7.2% (EOU-S). To ensure proper fitting within the impedance tube (inner diameter 28.6 mm), PTFE tape is applied circumferentially to compensate for dimensional reduction. Overall, OST samples show slightly lower diameter shrinkage, but higher thickness shrinkage compared with EOU, which is consistent with their generally higher bulk density and the less-developed mycelial network observed

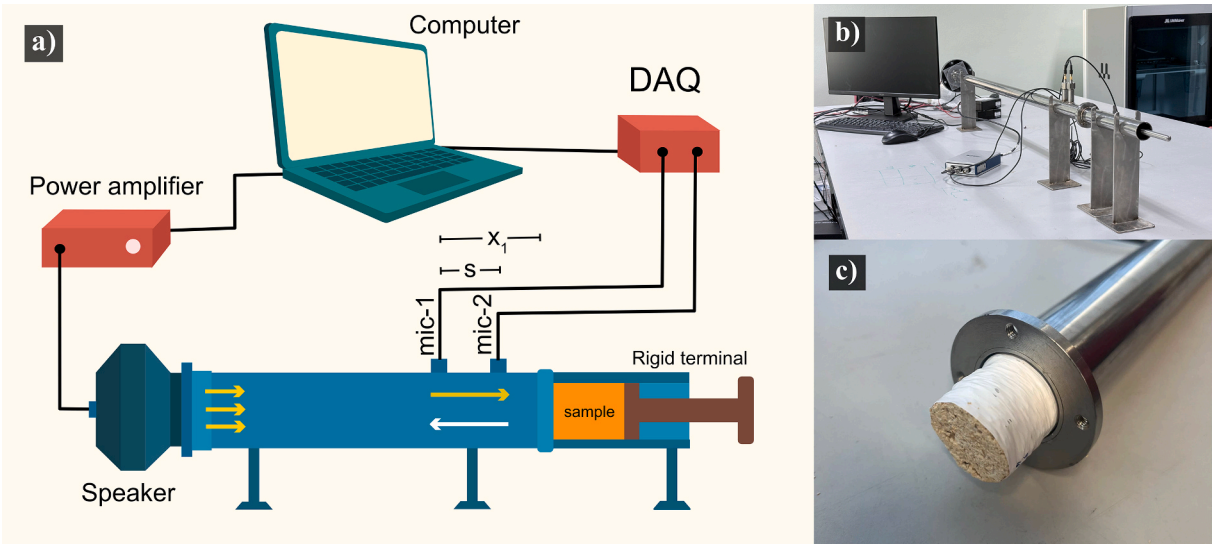

Fig. 2. The setup of the two-microphone impedance tube system used for SAC measurement a) schematic diagram, b) the actual image and c) cylindrical sample in the sample holder.

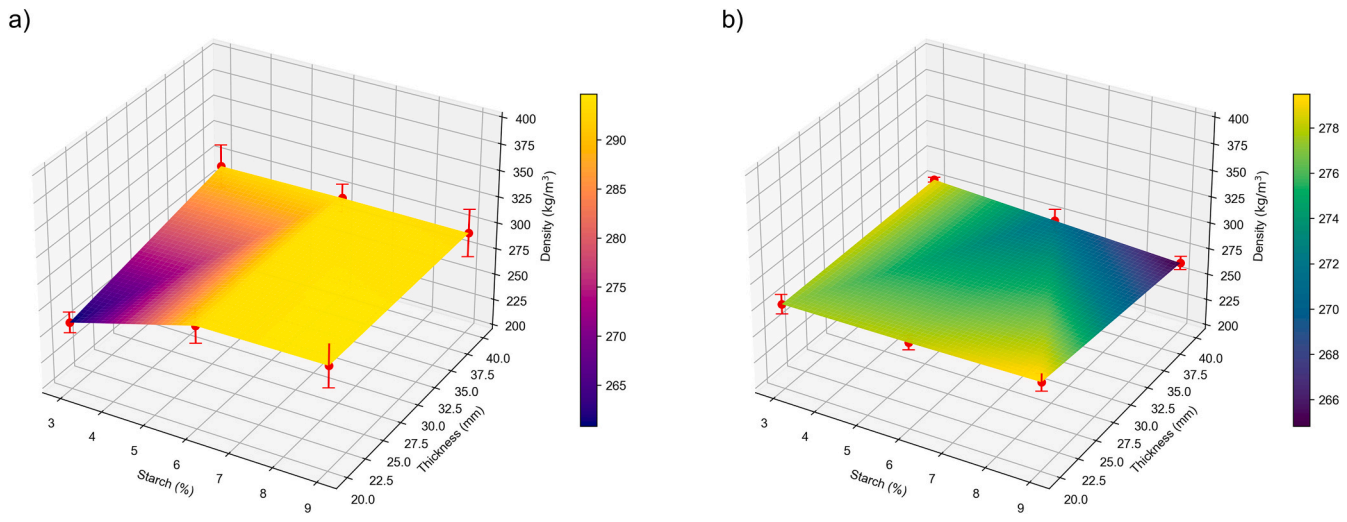

Fig. 4. Interpolated surface plots showing the average bulk density distribution of a) OST and b) EOU samples.

in the SEM images (Fig. 6), suggesting species-dependent drying behavior and microstructural control over shrinkage anisotropy.

To visualize the combined influence of two independent variables on a given response, a three-dimensional (3D) surface plot is used [42]. This representation simultaneously illustrates the dependence of the response variable on both independent parameters. Fig. 4 presents the 3D surface plots of density (kg/m^3) as a function of starch content (3–9%) and sample thickness (20–40 mm) for MBCs derived from (a) OST and (b) EOU. The red markers with error bars denote the measured means and standard deviations, which remain relatively small, indicating good experimental repeatability. Although density is theoretically independent of thickness, OST exhibits a systematic increase in apparent density with both increasing starch content and thickness, with values ranging from approximately 265 to 295 kg/m^3. This thickness-dependent trend is most pronounced at the lowest starch content and becomes less evident at higher starch levels. Given the small standard deviations, this behavior is unlikely to arise from random compaction inconsistencies and may instead reflect thickness-dependent drying behavior, as moisture removal and shrinkage can vary with sample thickness. This behavior suggests enhanced matrix consolidation or reduced pore volume, The lowest density occurs at 3% starch and 20 mm thickness, while the highest values are reached at 9% starch and 40 mm thickness. This thickness-related trend likely reflects differences in internal packing or growth compactness induced during processing rather than a true bulk density effect. In contrast, EOU displays a flatter and more uniform density surface plot, with values confined to a narrower range (~266–278 kg/m^3). A slight increase is observed at higher starch contents for thinner samples, while density remains nearly constant at greater thicknesses, which is consistent with the minimal peak shifting observed in the SAC spectra and indicates a more stable pore structure that is less sensitive to starch addition. Although direct microstructural evidence across all formulations is unavailable, the consistent correlation between density evolution and acoustic response supports a starch-induced modification of internal packing rather than random variability.

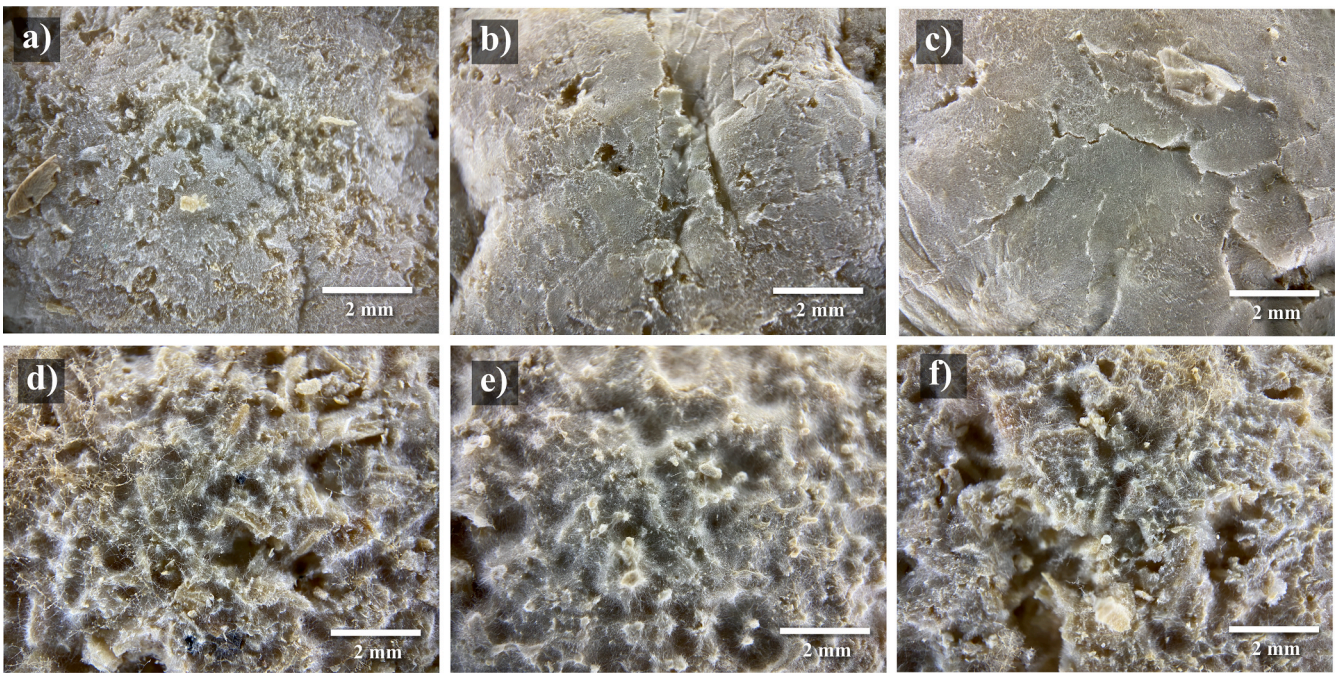

Fig. 5. Optical microscopic (OM) images showing surface morphology of MBCs which are a) OST-1 L b) OST-2 L c) OST-3 L d) EOU-1 L e) EOU-2 L and f) EOU-3 L.

3.2. Microscopic morphology

The OM images of the MBCs, shown in Fig. 5, provide a detailed view of the surface features of the two samples. The surface of the OST is notably smoother and more compact than EOU, with fewer irregularities and voids, indicating a tightly interwoven mycelial network. In contrast, EOU reveal a rougher surface with prominent porosity and uneven textures. These differences are attributed to the inherent morphological traits of the fungal species and their growth dynamics within the substrate.

Further examination of the surface of the samples using SEM confirms the optical observations and provides insight into the microstructure of the MBCs. Optical microscopy images (Fig. 5(a)–(c)) show that OST exhibits a more consolidated and less porous structure. These features are further confirmed by SEM analysis performed using a Hitachi SU3900 SEM (Hitachi High-Tech, Tokyo, Japan). As shown in Fig. 6(a), OST display a neat and continuous surface with a dense hyphal network, indicating compact mycelial growth. In contrast, the SEM images of EOU (Fig. 6(b)) reveal a more porous structure characterized by interconnected voids and irregularities. The hyphae of OST are denser and thicker than those of EOU, with average hyphal diameters of 16.67 μm and 13.8 μm, respectively. Both strains exhibited frequent mycelial collapse, which was associated with the mycelial characteristics of each strain.

At the microstructural level, the distinct morphologies of the two species imply different acoustic dissipation mechanisms. The higher porosity and well-interconnected pore network observed in EOU samples indicate a material with a more open structure, enabling effective sound wave penetration into the matrix. In contrast, the denser and more consolidated hyphal structure of the OST samples is likely to restrict acoustic energy penetration into the material [43–46], thereby favoring sound reflection over absorption. Moreover, the finer hyphal diameter of EOU samples (13.8 μm) may contribute to a more complex pore network compared to the thicker, more compact hyphae of OST.

3.3. Sound absorption coefficient

The SAC spectra at the 1/3 octave band frequencies between 200—5000 Hz of OST samples with thicknesses of 20 mm and 40 mm are presented in Fig. 7(a) and Fig. 7(b), respectively. These spectra offer a comparison of sound absorption behaviors across different thicknesses, providing valuable insights into how thickness influences acoustic performance.

In the low-frequency region, below 500 Hz, the SAC spectra for both 20 mm and 40 mm thick samples appear almost identical, indicating minimal effect of thickness on sound absorption at lower frequencies. However, as the frequency increases into the medium and high-frequency ranges, the SAC of the 40 mm thick samples shows notably

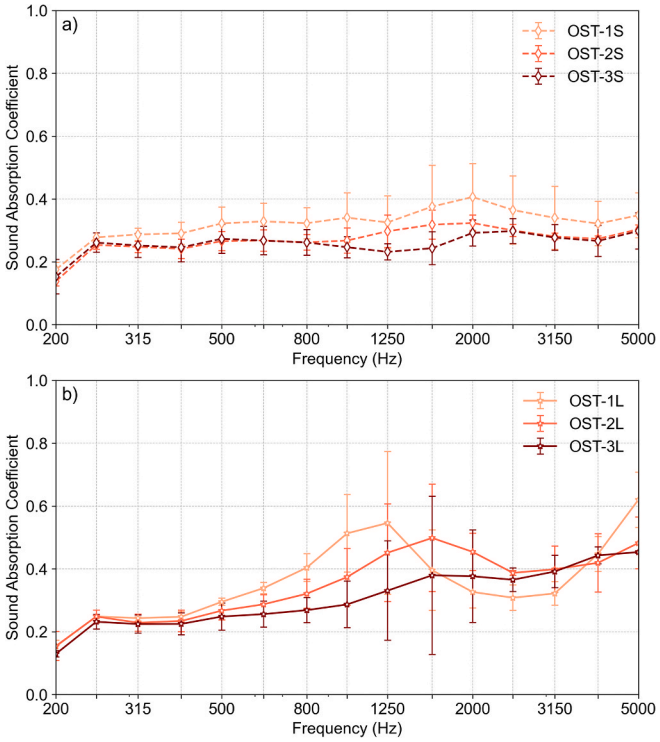

Fig. 7. SAC spectra of MBCs made from *P. ostreatus* (OST) with thicknesses of a) 20 mm and b) 40 mm.

higher values than those of the 20 mm thickness, suggesting that greater thickness enhances sound absorption at these frequencies. For the 20 mm thick samples (OST-1S ~ OST-3S), there is no notable difference in the SAC spectra across varying starch percentages, demonstrating that starch content does not substantially affect sound absorption in thinner samples. In contrast, for the 40 mm thick samples, the absorption peaks vary noticeably. OST-1 L exhibits the highest peak at approximately 1250 Hz, but as the starch percentage increases, the SAC peaks become lower, and the frequency at which the peak occurs shifts to higher values.

The SAC spectra of EOU samples with thicknesses of 20 mm and 40 mm are illustrated in Fig. 8(a) and Fig. 8(b), respectively. The maximum SAC values observed are around 0.62 for the 20 mm thick EOU-3S sample and 0.7 for the 40 mm thick EOU-3 L sample, indicating a slight improvement in sound absorption with increased thickness.

In general, for EOU the SAC spectra for the 40 mm thick samples are slightly higher than those for the 20 mm thick samples. All samples with 20 mm thickness demonstrate absorption peaks at around 1250 Hz.

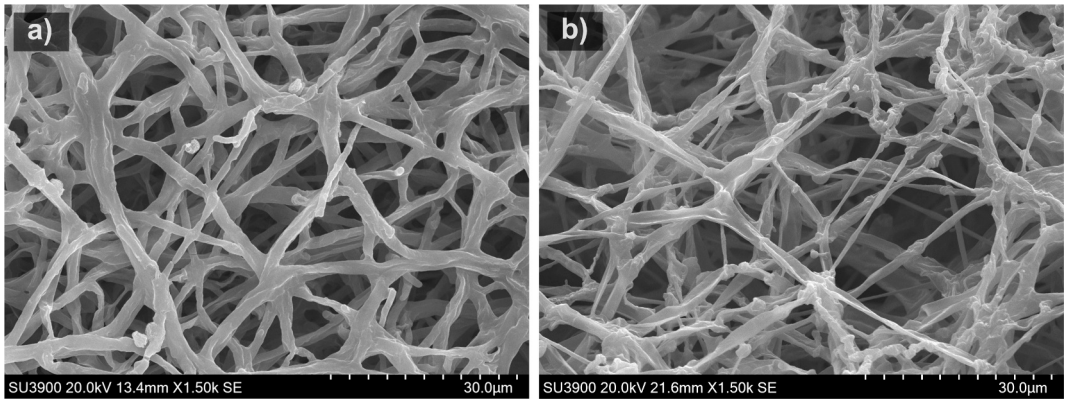

Fig. 6. Scanning electron microscope (SEM) images showing surface morphology of MBCs made from a) *P. ostreatus* and b) *P. eous*.

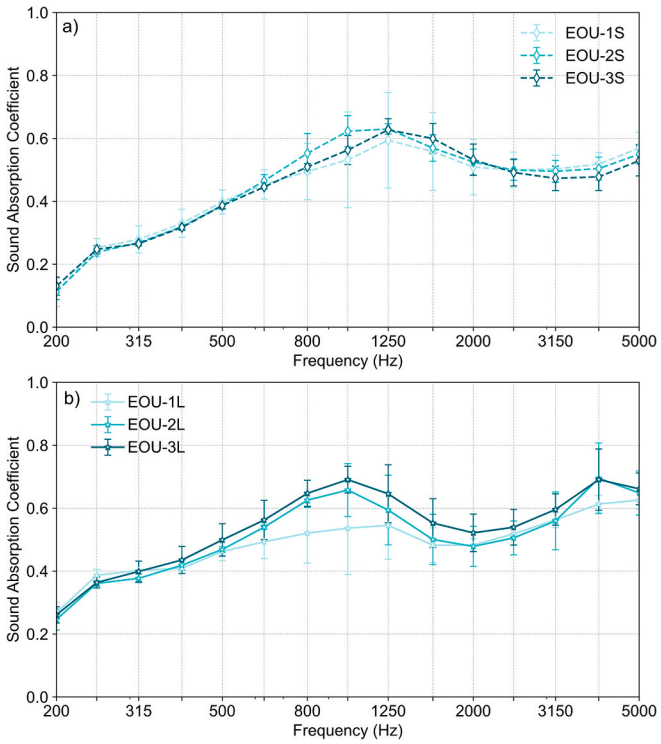

Fig. 8. SAC spectra of MBCs made from *P. eous* (EOU) with thicknesses of a) 20 mm and b) 40 mm.

Additionally, the SAC spectra for the 40 mm thick samples exhibit two peak points at 1000 Hz and 4000 Hz, a characteristic typically seen in porous structures with high thickness such as palmyra palm or water hyacinth [15]. This further supported the idea that increased thickness affects the absorption behavior at different frequencies. For the 20 mm thick samples (EOU-1S ~ EOU-3S), there is no notable variation in SAC spectra across different starch percentages, indicating that starch content has little impact on sound absorption in these thinner samples. On the other hand, in the 40 mm thick samples, the SAC peaks vary depending on the starch content. EOU-3 L, with the highest starch content, displays the highest peak at around 1000 Hz, while samples with lower starch content exhibit lower absorption peaks. According to Fig. 7 and Fig. 8, the SAC spectra of EOU show higher values compared to OST. This enhanced sound absorption can likely be attributed to the presence of clearly visible pores in the EOU [15,17,45]. The SAC spectra of EOU are higher across most frequency ranges compared with those of OST. In contrast, thinner OST samples exhibit relatively flat SAC curves, which coincide with the more compact surface morphology observed in microstructural imaging [15,17,47,48].

Changes in sound absorption can be qualitatively interpreted in relation to starch-induced microstructural evolution observed in the OM (Fig. 5) and SEM (Fig. 6) images. For OST samples, OM images (Fig. 5 (a)–(c)) show progressive surface densification with increasing starch content, as the growing mycelium increasingly covers and obscures the underlying substrate. This densified surface morphology coincides with the corresponding SAC spectra, which become flatter and exhibit a shift of the absorption peak toward higher frequencies. Such spectral changes may reflect alterations in pore connectivity and air transport pathways within the material [43,45,47], possibly linked to microstructural modifications associated with increased hyphal coverage. In contrast, the OM images of EOU samples (Fig. 5(d)–(f)) do not show pronounced surface densification with increasing starch content, and the substrate remains more visible than OST samples, reflecting the lower hyphal density. Consistent with this observation, the SAC spectra of EOU samples do not show an evident systematic peak shift across starch contents, which may imply a comparatively limited influence of starch addition on the effective pore structure. While the interpretations remain qualitative, the combined OM, SEM, and acoustic findings indicate a possible species-dependent response, reflected in differences in peak position and overall spectral shape.

Consider the single number to indicate the level of sound absorption, the NRC is defined as the arithmetic mean of the SAC values at 250, 500, 1000, and 2000 Hz [49]. Sound absorption average at low frequency (α_L) is calculated using the 1/3 octave band frequencies between 200——400 Hz. Rather than only reflecting geometric effects, the observed trends can be interpreted in terms of microstructural evolution. The consistent increase in NRC and α values with thickness across all frequency ranges reflects the longer effective propagation path within the porous network. For medium frequency (α_M), it will be calculated using 1/3 octave band frequencies between 500——1600 Hz. For high frequency (α_H), it is calculated using 1/3 octave band frequencies between 2000——5000 Hz [50,51]. Fig. 9 presents the 3D surface plots of NRC, α_L, α_M, and α_H for OST as functions of starch content (3–9%) and thickness (20–40 mm). Rather than only reflecting geometric effects, the observed trends can be interpreted in terms of microstructural evolution. The consistent increase in NRC, α_L, α_M, and α_H with thickness across all frequency ranges reflects the longer effective propagation path within the porous network [43,48], which enhances energy dissipation during sound propagation through the material [44–47]. This thickness dependence is most pronounced at high frequencies (α_H), where dissipation is dominated by pore-scale interactions near the surface [45,47].

At a fixed thickness, increasing starch content is associated with a systematic reduction in absorption performance. Based on the OM and SEM observations (Figs. 5 and 6), higher starch content appears to correspond to increased solid-phase presence (denser hyphal coverage) and partial obstruction of interconnected pores, which may contribute to a reduction in effective open porosity. Consequently, the combination of low starch (3%) and high thickness (40 mm) produces the most favorable balance between pore openness and structural continuity, yielding the highest NRC and α_M, whereas high starch (9%) and low thickness (20 mm) result in the poorest NRC, α_M and α_H.

Fig. 10 presents the corresponding 3D surface plots of NRC, α_L, α_M, and α_H for EOU. In contrast to OST, the EOU surfaces indicate that sound absorption metrics are primarily governed by sample thickness, with no clear monotonic increase or decrease associated with starch content across the investigated range. At both 20 and 40 mm, NRC and frequency-averaged absorption values remain relatively insensitive to starch variation, whereas increasing thickness consistently enhances absorption at most frequency ranges.

Although OST exhibits a relatively smoother surface morphology, OM and SEM images (Figs. 4–5) suggest that EOU may possess a higher apparent volume of open pores. This structural difference could partially explain the comparatively higher NRC and broader-band absorption observed for EOU samples [16,17,50]. This observation is consistent with the surface plots, which show no clear starch-dependent trend in NRCs or frequency-averaged absorption for EOU samples. In contrast, the acoustic performance of OST exhibit greater sensitivity to starch content. Starch in OST sample is assumed to function primarily as a nutrient that promotes mycelial growth, leading to denser hyphal networks and altered pore connectivity as shown in Fig. 5. These species-dependent growth responses result in measurable changes in acoustic behavior for OST, whereas EOU maintains a porous-dominated response largely independent of starch variation. While these trends are evident from the surface plots and microstructural observations, the statistical significance of thickness, starch content, and their interaction effects is quantitatively evaluated using ANOVA, as presented in Subsection 3.5.

3.4. *Compressive strength Tests*

The mechanical response of the MBCs under compressive loading

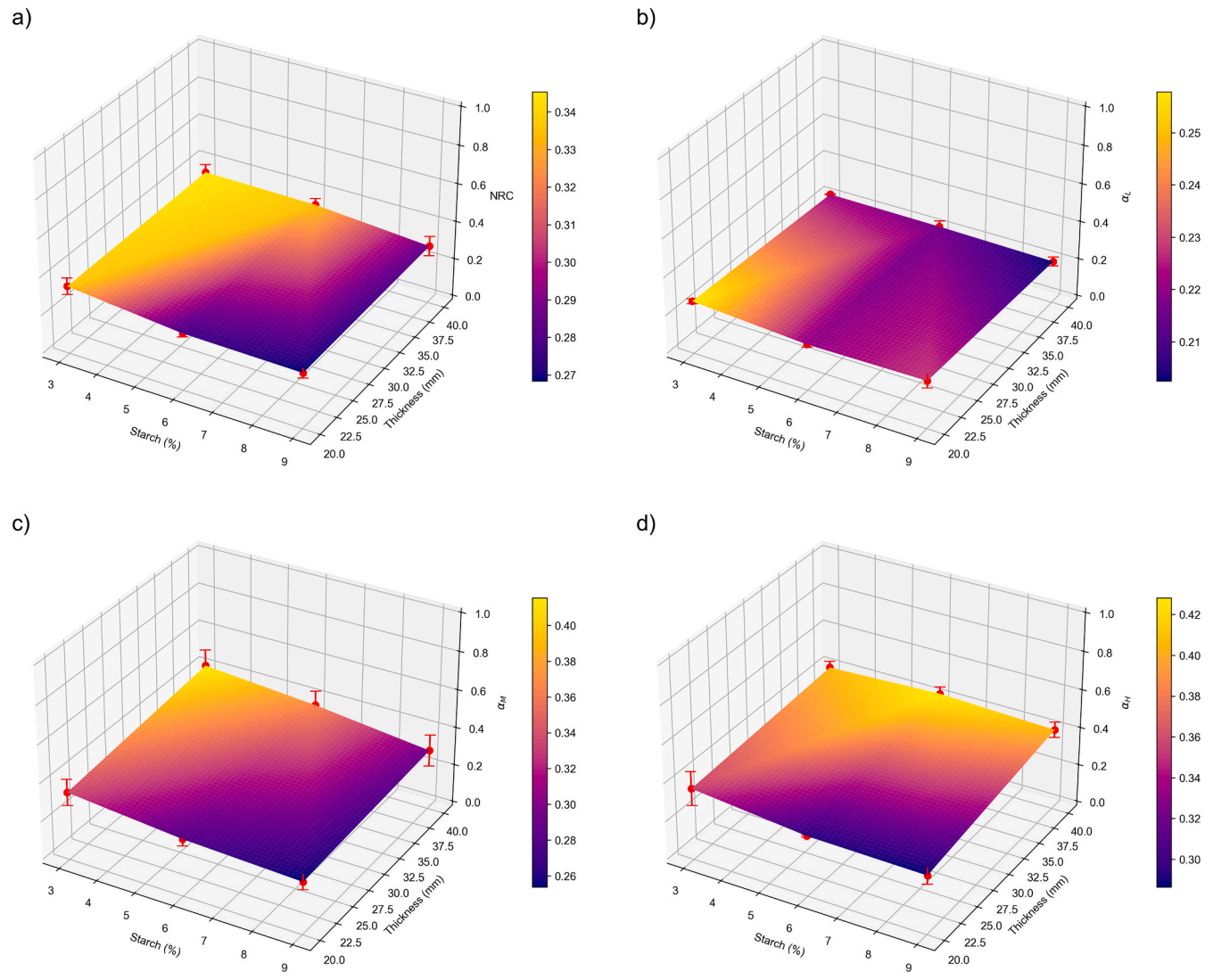

Fig. 9. Interpolated surface plots of the average acoustic parameters OST samples: a) NRC, b) α_L c), α_M, and d) α_H.

reveals clear species-dependent differences that are relevant to their acoustic performance. The stress–strain behavior shows a well-defined elastic region followed by yielding, with yield strength determined using the 0.2% offset method as shown in Fig. 11(a). Due to the fixed specimen length of 20 mm, ultimate compressive failure was not reached during testing. Across all formulations, OST exhibit consistently higher stiffness and strength than EOU, indicating a mechanically more consolidated material system. Quantitatively, OST samples display higher elastic modulus values (171.2–221.2 kPa) than EOU samples (109.2–163.1 kPa), with the difference being statistically significant ($p = 0.0094$), as shown in Fig. 11(b). Similarly, OST shows higher yield strength (19.6–24.3 kPa) compared to EOU (12.0–13.8 kPa), a distinction that is highly significant ($p = 9.74 \times 10^{-5}$), as shown in Fig. 11(c). These results confirm that OST forms a stiffer and mechanically stronger network, likely due to higher hyphal density and a more compact microstructure observed in the OM and SEM images (Figs. 5 and 6).

The mechanically stronger behavior of the OST samples, consistent with the denser and less porous microstructure observed in the OM and SEM images, may reduce sound absorption by limiting effective acoustic penetration into the pore network [44,45,47]. In contrast, the lower stiffness and yield strength of the EOU samples are consistent with a more compliant and porous structure, which promotes greater interaction between incident sound waves and the internal pore structure, albeit with reduced load-bearing capacity.

These results highlight an inherent trade-off between mechanical strength and acoustic performance in mycelium-based composites. While OST may be better suited for applications requiring higher stiffness and structural integrity, most EOU samples offer higher SAC spectra across frequencies ranges due to their lower stiffness and higher porosity. If structural–acoustic multifunctionality is desired, these findings suggest that species selection and processing parameters must be carefully balanced to achieve an optimal compromise between mechanical performance and sound absorption.

3.5. Statistical analysis

In Table 2, a two-way analysis of variance (ANOVA) was performed to evaluate the effects of starch content (3, 6, and 9%) and specimen thickness (20 and 40 mm) on the density, NRC, the average of SAC at low (α_L), medium (α_M), and high (α_H) frequencies. Both factors were treated as categorical variables, and their interaction was included in the model. The analysis was carried out using the ordinary least squares (OLS) framework implemented in the statsmodels package (Type II sum of squares) in Python. Normality of residuals was verified using the Shapiro–Wilk test, and for responses showing significant starch effects, Tukey's HSD post-hoc comparisons were conducted for some parameters. These analyses clarify how starch content and thickness jointly influence the acoustic performance of the MBCs prepared from

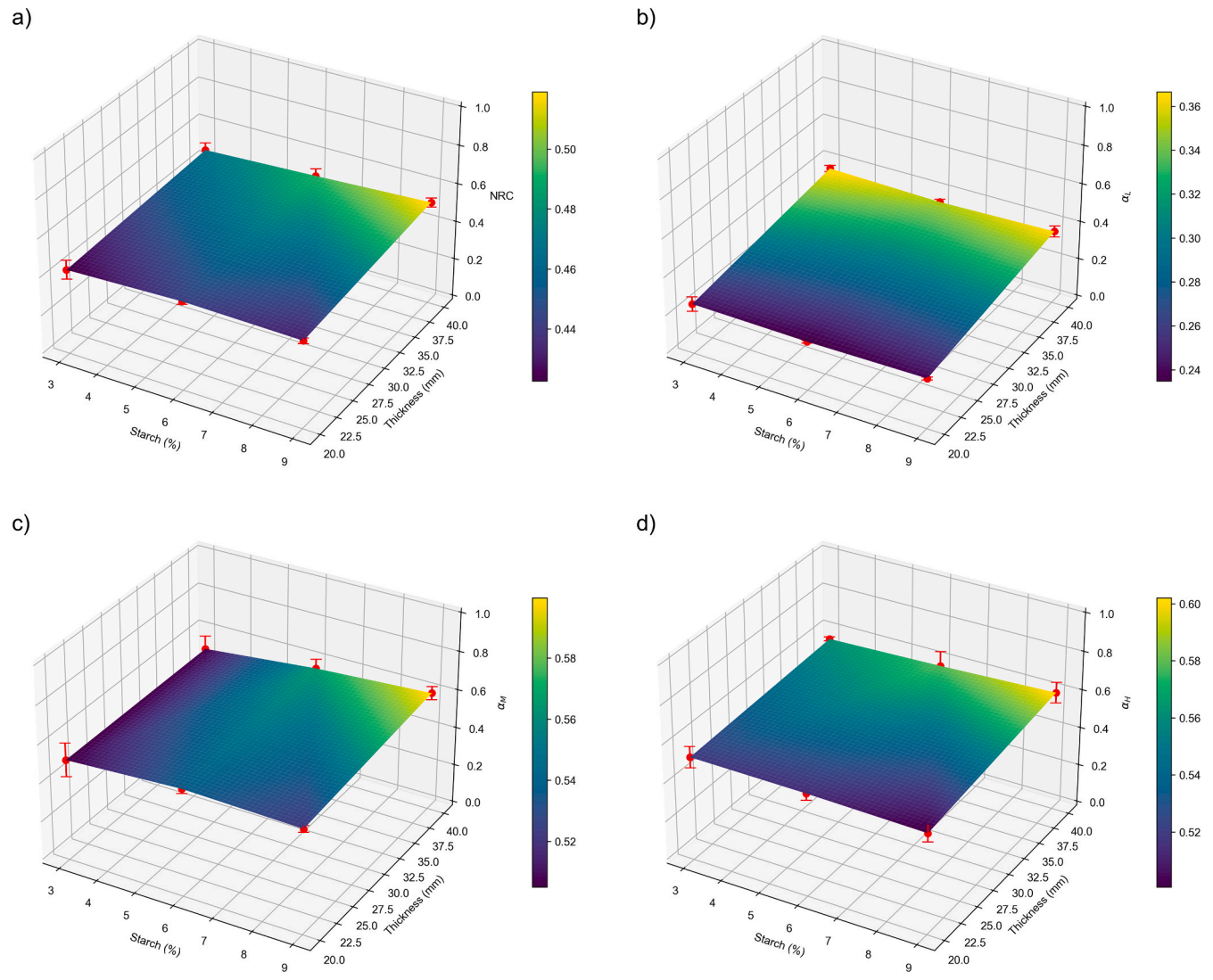

Fig. 10. Interpolated surface plots of the average acoustic parameters EOU samples: a) NRC, b) α_L c), α_M, and d) α_H.

P. ostreatus and *P. eous*.

For density, neither starch content nor thickness shows a statistically significant effect in OST samples, and no interaction between factors is detected. The moderate explanatory power of the model ($R^2 = 0.426$) indicates that, while the tested factors account for a portion of the variability, a substantial fraction remains unexplained, suggesting the influence of additional microstructural or processing-related variables. A similar pattern is observed for EOU, where thickness approaches but does not reach statistical significance ($p = 0.099$), and the model explains 40.8% of the variance. Taken together, these results suggest that starch modification has a limited practical impact on bulk density for both species, with any thickness-related effects in EOU being comparatively small and uncertain within the experimental variability.

In contrast, NRC exhibits clear species-specific behavior. For OST samples, starch content has a statistically significant effect ($p = 0.039$), with Tukey's HSD indicating a reduction in NRC at higher starch levels, whereas thickness shows no measurable influence. Although significant, the overall explanatory power of the model is moderate ($R2 = 0.509$), indicating that starch-related changes account for only part of the observed variability in NRC. Conversely, for EOU, starch content is not significant, while thickness exerts a strong influence on NRC ($p = 0.003$). The higher R2 value for EOU (0.618) suggests that thickness has a more substantial and practically meaningful role in governing NRC for this species.

For low-frequency absorption (α_L), OST shows no statistically significant dependence on either starch content or thickness, indicating limited practical sensitivity to these parameters in this frequency range. In contrast, EOU exhibits a highly significant thickness effect ($p < 0.001$), with thickness accounting for approximately 92% of the total variance ($R^2 = 0.920$). This strong explanatory power confirms thickness as the dominant and practically relevant factor controlling low-frequency absorption in EOU. This behavior is consistent with the more porous microstructure of EOU, which allows deeper sound penetration into the material. Conversely, the denser and more consolidated structure of OST likely restricts low-frequency wave propagation, thereby limiting the effectiveness of thickness variation in this frequency band.

The α_M shows species-dependent but statistically insignificant responses to the tested factors. For OST, both starch content and thickness exhibit p-values greater than 0.05, although they are marginally closer to the significance threshold than those observed for EOU, indicating weak formulation-dependent tendencies. The moderate coefficient of determination ($R^2 = 0.497$) suggests that these factors account for a limited yet non-negligible portion of the variability in α_M. In contrast, for EOU, the p-values associated with starch content and thickness are substantially higher than 0.05, and the lower R^2 value (0.378) indicates that α_M is only weakly related to the tested parameters. This reduced explanatory power implies that specimen-to-specimen variability and

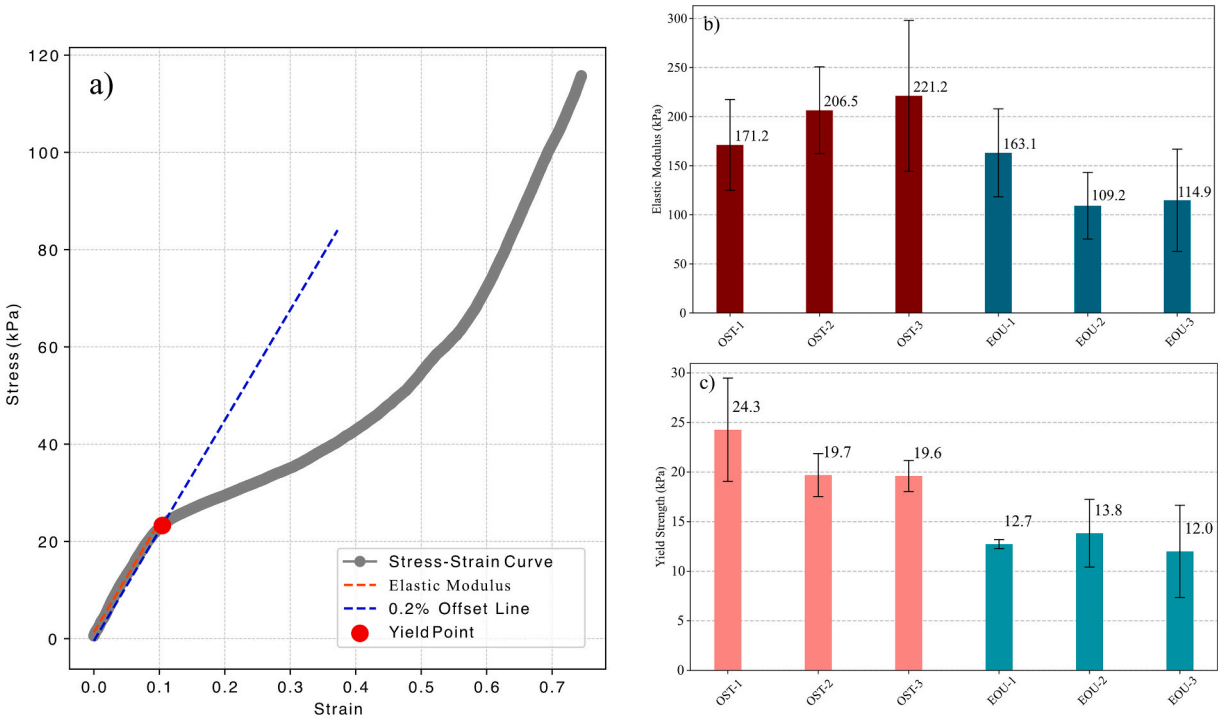

Fig. 11. Mechanical properties of OST and EOU samples a) compressive stress–strain curve, b) compressive elastic modulus and c) yield strength.

Table 2
ANOVA results (p-values) for the effects of starch and thickness on density and other physical properties in OST and EOU.

variable	starch	thickness	starch × thickness	R-squared	CV (%)
OST-based (*P. ostreatus*)					
Density	0.180	0.235	0.225	0.426	6.9
NRC	0.039*	0.144	0.509	0.509	14.7
α_L	0.169	0.077	0.523	0.436	11.7
α_M	0.068	0.051	0.823	0.497	24.7
α_H	0.490	0.001**	0.313	0.659	19.3
Elastic modulus	0.581	–	–	0.165	27.4
Yield strength	0.235	–	–	0.383	17.6
EOU-based (*P. eous*)					
Density	0.433	0.099	0.236	0.408	3.1
NRC	0.281	0.002**	0.490	0.618	9.6
α_L	0.614	<0.001**	0.935	0.920	21.8
α_M	0.199	0.182	0.474	0.378	10.4
α_H	0.928	0.013*	0.587	0.446	10.4
Elastic modulus	0.330	–	–	0.309	35.7
Yield strength	0.802	–	–	0.071	23.4

Note: * and ** denote statistical significance at $p \leq 0.05$ and $p \leq 0.01$, respectively.

other uncontrolled microstructural or processing-related factors dominate the response. Overall, while OST exhibits slightly stronger formulation-related trends than EOU, a large fraction of the variability remains unexplained for both species. For α_H, thickness emerges as a key determinant in both species. OST shows a strong thickness effect ($p = 0.001$, $R^2 = 0.659$), while in EOU, thickness is also significant ($p = 0.013$) but with a lower R^2 (0.446), indicating moderate explanatory power. These findings confirm that increasing thickness enhances high-frequency absorption consistently across both species, although the effect is more pronounced in OST.

For mechanical properties, one-way ANOVA was applied to assess the effect of starch content on elastic modulus and yield strength. In both species, starch content shows no statistically significant influence on either property. For OST, the models explain only a small proportion of the variance ($R^2 = 0.165$ for elastic modulus and 0.383 for yield strength). For EOU, the explanatory power is similarly limited, with a slightly higher R^2 for elastic modulus (0.309) but a markedly lower R^2 for yield strength (0.071). These low R^2 values indicate that starch content has a limited practical impact on mechanical performance under the tested conditions. Importantly, this suggests that starch-based acoustic tuning does not measurably compromise the mechanical stability of either species.

3.6. Comparative studies

The sound absorption performance of mycelium-based composites in this study was compared with previous findings reported by Jinanukul *et al.* [52] and Walter and Gürso [53], as presented in Table 3. The comparison highlights the influence of fungal species, substrate composition, material density, and thickness on the SAC across different frequencies. It should be noted that direct quantitative comparison of SAC values across studies should be interpreted with caution, as SAC is strongly affected by specimen thickness.

The results show that the SAC values of OST and EOU from this study

Table 3
Comparative studies of sound absorbing performance of OST and EOU compared to other fungal species.

Fungal Species	Substrate	Density (kg/m^3)	Thickness (mm)	250 Hz	500 Hz	1 kHz	Reference
P. ostreatus	74% sawdust	260	20	0.28	0.32	0.34	This study
P. eous	74% sawdust	277	20	0.25	0.40	0.53	This study
L. sajor-caju	100% corn husk	~210	24	0.4	0.34	0.85	Jinanukul *et al.* [52]
L. sajor-caju	75% corn husk, 25% sawdust	~212	24	0.51	0.49	0.94	Jinanukul *et al.* [52]
L. sajor-caju	50% corn husk, 50% sawdust	~230	24	0.43	0.45	0.86	Jinanukul *et al.* [52]
L. sajor-caju	25% corn husk, 75% sawdust	~243	24	0.43	0.43	0.84	Jinanukul *et al.* [52]
L. sajor-caju	100% sawdust	~255	24	0.4	0.41	0.61	Jinanukul *et al.* [52]
P. ostreatus	shredded cardboard	325	25	0.16	0.51	0.69	Walter & Gürso [53]
P. ostreatus	fine cardboard	375	25	0.21	0.51	0.47	Walter & Gürso [53]

are higher than those of the cardboard-based MBCs studied by Walter and Gürso [53], particularly at 1000 Hz (1 kHz), where the shredded and fine cardboard samples recorded SAC values of 0.69 and 0.47, respectively. In contrast, EOU samples in this study achieved 0.53 at 1000 Hz, demonstrating a competitive absorption performance despite the differences in substrate type. However, the SAC values in this study are lower than those of *Lentinus sajor-caju* samples reported by Jinanukul *et al.* [52], which exhibit the highest absorption at 1000 Hz, ranging from 0.61 to 0.94 depending on the proportion of corn husk and sawdust as substrates. One key factor affecting the absorption performance is the thickness of the samples. The samples in this study are 20 mm thick, whereas those from Jinanukul *et al.* [52] are 24 mm thick, and those from Walter and Gürso [53] are 25 mm thick. Since sound absorption is directly influenced by material thickness—where thicker materials generally absorb more sound, particularly at low frequencies—it is expected that the SAC values in this study would be lower. However, an interesting finding is that despite having lower thickness, the current samples still achieve higher SAC values than the cardboard-based samples from Walter and Gürso [53], indicating that substrate composition plays a more critical role than thickness alone in determining sound absorption performance.

The SAC values of the mycelium-based composites investigated in this study fall within the range reported for bio-based porous absorbers at comparable thicknesses. Although the specimens are slightly thinner, the measured SAC values, particularly at 1000 Hz for the EOU samples, are comparable to those reported by Jinanukul *et al.* and do not indicate clear performance superiority. Accordingly, differences in octave-band SAC are discussed in terms of formulation-dependent trends and experimental variability, not small thickness variations. These results suggest that substrate composition and growth conditions influence acoustic response, warranting further systematic investigation.

While this study establishes a species-dependent acoustic response, further research is required to evaluate the long-term durability of these composites under realistic service conditions. A critical priority is the characterization of fire reaction properties via standardized methodology to quantify ignition delay, peak heat release rates (pHRR), and smoke production yields [27]. Specific investigation is needed into the char-forming mechanisms [54] of the surface mycelium saples; for instance, determining how the 20 mm and 40 mm thicknesses used in this study influence the char-layer stability and oxygen-barrier efficiency. Furthermore, given the hygroscopic nature of fungal biomass, the impact of moisture absorption and thermal cycling on fire-retardant performance must be assessed [27,54]. Future iterations should also explore additives to enhance the condensed-phase flame retardancy, alongside a life cycle assessment (LCA) to benchmark these bio-based materials against conventional petroleum-derived foams for integration into sustainable prefabricated building systems.

4. Conclusion

Mycelium-based composites (MBCs) derived from *Pleurotus ostreatus* (OST) and *Pleurotus eous* (EOU) are viable, sustainable alternatives for acoustic applications, with their performance dictated by distinct species-dependent microstructures. EOU exhibited higher sound absorption, reflected by higher noise reduction coefficient (NRC) values, which is associated with its finer hyphal diameter (13.8 μm) and a more porous structure. Conversely, OST exhibited a denser, more consolidated network with thicker hyphae (16.67 μm), resulting in notably higher compressive yield strength and stiffness but lower sound absorption. ANOVA indicated that thickness is the dominant factor influencing the NRC and the average sound absorption at low and high frequency ranges for EOU samples, whereas starch content showed an effect on the NRC of OST samples. Importantly, the study found that acoustic optimization via starch content does not compromise mechanical integrity, as the yield strength of both species remained unaffected by varying starch levels. Ultimately, these findings provide a foundation for species-driven design, suggesting that EOU shows potential for enhanced sound absorption, while OST offers a balanced solution for multifunctional, semi-structural building components in green construction.

CRediT authorship contribution statement

Tanyaporn Damthip: Writing – review & editing, Writing – original draft, Validation, Methodology, Investigation, Formal analysis, Data curation. **Nur-asrin Hama:** Writing – review & editing, Writing – original draft, Validation, Methodology, Investigation, Formal analysis, Data curation. **Sakchai Khongnakhon:** Writing – review & editing, Supervision, Investigation, Formal analysis. **Benjawan Yanwisetpakdee:** Writing – review & editing, Writing – original draft, Supervision, Investigation, Formal analysis. **Polphat Ruamcharoen:** Writing – review & editing, Validation, Supervision, Methodology, Investigation, Formal analysis. **Purintorn Chanlert:** Writing – review & editing, Writing – original draft, Visualization, Validation, Supervision, Software, Resources, Project administration, Methodology, Investigation, Funding acquisition, Formal analysis, Data curation, Conceptualization.

Declaration of competing interest

The authors declare that they have no known competing financial interests or personal relationships that could have appeared to influence the work reported in this paper.

Acknowledgement

The authors would like to thank the Faculty of Science and Technology, Songkhla Rajabhat University, for providing the equipment and laboratory facilities necessary to carry out this research. Part of this work is currently in the process of Thailand's petty patent registration under the request number 2503002919.

Data availability

Data will be made available on request.

References

[1] Worrell E, Price L, Martin N, Hendriks C, Meida LO. Carbon Dioxide Emissions from the Global Cement Industry. Annu Rev Energy Env 2001;26:303–29. https://doi.org/10.1146/annurev.energy.26.1.303.

[2] Abera YA. Sustainable building materials: a comprehensive study on eco-friendly alternatives for construction. Compos Adv Mater 2024;33:26349833241255957. https://doi.org/10.1177/26349833241255957.

[3] Nußholz JLK, Nygaard Rasmussen F, Milios L. Circular building materials: Carbon saving potential and the role of business model innovation and public policy. Resour Conserv Recycl 2019;141:308–16. https://doi.org/10.1016/j.resconrec.2018.10.036.

[4] Dsilva J, Zarmukhambetova S, Locke J. Assessment of building materials in the construction sector: a case study using life cycle assessment approach to achieve the circular economy. Heliyon 2023;9:e20404. https://doi.org/10.1016/j.heliyon.2023.e20404.

[5] Berardi U, Iannace G. Predicting the sound absorption of natural materials: Best-fit inverse laws for the acoustic impedance and the propagation constant. Appl Acoust 2017;115:131–8. https://doi.org/10.1016/j.apacoust.2016.08.012.

[6] Zhou B, Zhang J, Li X, Liu B. An investigation on the sound absorption performance of granular molecular sieves under room temperature and pressure. Materials 2020;13:1–12. https://doi.org/10.3390/MA13081936.

[7] Martwong E, Yingshataporn-a-nan T, Minanandana T, Puksuwan K, Junthip J, Sukhawipat N. Sound absorption and thermal insulation materials from waste palm oil for housing application: Green polyurethane/water hyacinth fiber sheet composite. Constr Build Mater 2024;438:137007. https://doi.org/10.1016/j.conbuildmat.2024.137007.

[8] Ehsan Samaei S, Berardi U, Asilian Mahabadi H, Soltani P, Taban E. Optimization and modeling of the sound absorption behavior of polyurethane composite foams reinforced with kenaf fiber. Appl Acoust 2023:202. https://doi.org/10.1016/j.apacoust.2022.109176.

[9] Buratti C, Merli F, Moretti E. Aerogel-based materials for building applications: Influence of granule size on thermal and acoustic performance. Energ Buildings 2017;152:472–82. https://doi.org/10.1016/j.enbuild.2017.07.071.

[10] Smirnova OM, de Navascués IMP, Mikhailevskii VR, Kolosov OI, Skolota NS. Sound-absorbing composites with rubber crumb from used tires. Applied Sciences (Switzerland) 2021;11:doi:10.3390/app11167347.

[11] SheikhMozafari MJ, Taban E, Soltani P, Faridan M, Khavanin A. Sound absorption and thermal insulation performance of sustainable fruit stone panels. Appl Acoust 2024;217:109836. https://doi.org/10.1016/j.apacoust.2023.109836.

[12] Seetapong N, Chorphakar N, Saenkuea N, Chulok S, Ruamcharoen P, Chanlert P. Sustainable Bio-based Composites from Termite Mound Soil and Agro-Waste for Lightweight and Acoustic applications. Trends Sci 2025;23:11507. https://doi.org/10.48048/tis.2026.11507.

[13] Kalasee W, Lakachaiworakun P, Eakvanich V, Dangwilailux P. Sound absorption of natural fiber composite from sugarcane bagasse and coffee silver skin. Journal of the Korean Wood Science and Technology 2023;51:470–80. https://doi.org/10.5658/WOOD.2023.51.6.470.

[14] Taban E, Soltani P, Berardi U, Putra A, Mousavi SM, Faridan M, et al. Measurement, modeling, and optimization of sound absorption performance of Kenaf fibers for building applications. Build Environ 2020;180:107087. https://doi.org/10.1016/J.BUILDENV.2020.107087.

[15] Srisawas M, Kerdkaew T, Chanlert P. From invasive species to bio-based composites: Utilizing water hyacinth for sound absorption and insulation. Ind Crop Prod 2024;220:119242. https://doi.org/10.1016/j.indcrop.2024.119242.

[16] Chanlert P, Ruamcharoen P, Kerdkaew T. Exploring the sound absorption and sound insulation capabilities of natural fiber composites: nipa palm peduncle fiber. Chiang Mai J Sci 2024;51:1–11. https://doi.org/10.12982/CMJS.2024.034.

[17] Chanlert P, Tongyoo S, Rordrak C. Effects of urea–formaldehyde and polyvinyl acetate adhesive on sound absorption coefficient and sound transmission loss of palmyra palm fruit fiber composites. Appl Acoust 2022;198:108984. https://doi.org/10.1016/j.apacoust.2022.108984.

[18] Chulok S, Auppawirot P, Bunpha M, Daoreung K, Seetapong N, Chanlert P. Tropical wood acoustics: impregnation effects on Cajuput, Mangium, and Mango woods for sustainable building materials. Eur J Wood Prod 2025;83:121. https://doi.org/10.1007/s00107-025-02274-4.

[19] Pop MA, Croitoru C, Matei S, Zaharia S-M, Coșniță M, Spîrchez C. Thermal and Sound Insulation Properties of Organic Biocomposite Mixtures. Polymers 2024;16:672. https://doi.org/10.3390/polym16050672.

[20] Masuda T, Takano K, Hiyama K, Osada T. Development of Sustainable Plant-based Sound-Absorbing Boards to Reduce Noise in Interior Spaces. Sustainability 2023;15:15230. https://doi.org/10.3390/su152115230.

[21] Yang L, Park D, Qin Z. Material Function of Mycelium-based Bio-Composite: a Review. Front Mater 2021;8. https://doi.org/10.3389/fmats.2021.737377.

[22] Khyaju S, Kuangharn T. Diverse use of mushroom mycelium-based as biomaterial products: a mini review. Fungal Biotec 2024;4:56–67. https://doi.org/10.5943/FunBiotec/4/1/4.

[23] Motamedi S, Rousse DR, Promis G. Mycelium as a building material: current status and development perspective,International Congress on Advanced Materials Sciences and Engineering (ASME2023), Vienna, Austria: 2023.

[24] Xia Q. Utilizing mycelium-based materials for sustainable construction. Applied and Computational Engineering 2024;63:10–5. https://doi.org/10.54254/2755-2721/63/20240967.

[25] Shin H-J, Ro H-S, Kawauchi M, Honda Y. Review on mushroom mycelium-based products and their production process: from upstream to downstream. Bioresour Bioprocess 2025;12:3. https://doi.org/10.1186/s40643-024-00836-7.

[26] Javadian A, Le Ferrand H, Hebel DE, Saeidi N. Application of mycelium-bound composite materials in construction industry. A Short Review SOJMSE 2020;7:1–9. https://doi.org/10.15226/sojmse.2020.00162.

[27] Jones M, Bhat T, Kandare E, Thomas A, Joseph P, Dekiwadia C, et al. Thermal degradation and Fire Properties of Fungal Mycelium and Mycelium - Biomass composite materials. Sci Rep 2018;8:17583. https://doi.org/10.1038/s41598-018-36032-9.

[28] Jones M, Bhat T, Wang CH, Moinuddin K, John S Thermal Degradation and Fire Reaction Properties of Mycelium Composites,21st International Conference on Composite Materials. Xi'an, China; 2017.

[29] Gezer ED, Uçar E, Gümüşkaya E. Physical and mechanical properties of mycelium-based fiberboards. BioRes 2024;19:3421–35. https://doi.org/10.15376/biores.19.2.3421-3435.

[30] Aiduang W, Kumla J, Srinuanpan S, Thamjaree W, Lumyong S, Suwannarach N. Mechanical, physical, and chemical properties of mycelium-based composites produced from various lignocellulosic residues and fungal species. JoF 2022;8:1125. https://doi.org/10.3390/jof8111125.

[31] Fletcher I, Freer A, Ahmed A, Fitzgerald P. Effect of temperature and growth media on mycelium growth of pleurotus ostreatus and ganoderma lucidum strains. Cohesive J Microbiol Infect Dis 2019;2:000549. https://doi.org/10.31031/CJMI.2019.02.000549.

[32] Telang SM, Patil SS, Baig MMV. Comparative study on yield and nutritional aspect of Pleurotus eous mushroom cultivated on different substrate. Food Sci Res J 2010;1:60–3.

[33] Jatwa T, Apet KT, Wagh SS, Sayyed KS, Rudrappa KB, Sornapriya SP. Evaluation of Various Agro-Wastes for Production of Pleurotus spp. (P. florida, P. sajor-caju and P. eous). J PURE APPL MICROBIO 2016;10:2783–92. doi:10.22207/JPAM.10.4.37.

[34] Elsacker E, Vandelook S, Brancart J, Peeters E, De Laet L. Mechanical, physical and chemical characterisation of mycelium-based composites with different types of lignocellulosic substrates. PLoS One 2019;14:e0213954. https://doi.org/10.1371/journal.pone.0213954.

[35] Lei H, Li L, Yang W, Bian Y, Li C-Q. An analytical review on application of life cycle assessment in circular economy for built environment. Journal of Building Engineering 2021;44:103374. https://doi.org/10.1016/j.jobe.2021.103374.

[36] Jones M, Mautner A, Luenco S, Bismarck A, John S. Engineered mycelium composite construction materials from fungal biorefineries: a critical review. Mater Des 2020;187:108397. https://doi.org/10.1016/j.matdes.2019.108397.

[37] Girometta C, Picco AM, Baiguera RM, Dondi D, Babbini S, Cartabia M, et al. Physico-Mechanical and Thermodynamic Properties of Mycelium-based Biocomposites: a Review. Sustainability 2019;11:281. https://doi.org/10.3390/su11010281.

[38] Chanlert P. Schematic representation of the mycelium brick sample preparation. Created in BioRender 2025. https://BioRender.com/2s941ke.

[39] American Society for Testing of Materials 1990. https://doi.org/10.1520/E1050-12.

[40] Part 2: Transfer-Function Method 1998. https://doi.org/10.3403/BSENISO10534.

[41] ASTM D695. Test Method for Compressive Properties of Rigid Plastics 2015. doi:10.1520/D0695-15.

[42] Dehdashti Z, Soltani P, Taban E. Utilizing discarded face masks to fabricate sustainable high-performance panels for enhanced building thermal and acoustic comfort. J Clean Prod 2024:446. https://doi.org/10.1016/j.jclepro.2024.141304.

[43] Allard JF, Atalla N. Propagation of Sound in Porous Media. Hoboken, New Jersey, USA: Wiley; 2009.

[44] Johnson DL, Koplik J, Dashen R. Theory of dynamic permeability and tortuosity in fluid-saturated porous media. J Fluid Mech 1987;176:379. https://doi.org/10.1017/S0022112087000727.

[45] Champoux Y, Allard JF. Dynamic tortuosity and bulk modulus in air-saturated porous media. J Appl Phys 1991;70:1975–9. https://doi.org/10.1063/1.349482.

[46] Allard JF, Champoux Y. New empirical equation for sound propagation in rigid frame fibrous materials. J Acoust Soc Am 1992;91:3346–53. https://doi.org/10.1121/1.402824.

[47] Champoux Y, Stinson MR. On acoustical models for sound propagation in rigid frame porous materials and the influence of shape factors. J Acoust Soc Am 1992;92:1120–31. https://doi.org/10.1121/1.405281.

[48] Delany ME, Bazley EN. Acoustical properties of fibrous absorbent materials. Appl Acoust 1970;3:105–16. https://doi.org/10.1016/0003-682X(70)90031-9.

[49] Reverberation Room Method 2009.

[50] Chulok S, Auppawirot P, Bunpha M, Daoreung K, Seetapong N, Chanlert P. Tropical wood acoustics: impregnation effects on Cajuput, Mangium, and Mango woods for sustainable building materials. Eur J Wood Wood Prod 2025. https://doi.org/10.1007/s00107-025-02274-4.

[51] Chanlert P, Jintara A, Manoma W. Comparison of the sound absorption properties of acoustic absorbers made from used copy paper and corrugated board. BioResources 2022;17:5612–21. https://doi.org/10.15376/biores.17.4.5612-5621.

[52] Jinanukul P, Kumla J, Aiduang W, Thamjaree W, Oranratmanee R, Shummadtayar U, et al. Comparative Evaluation of Mechanical and Physical Properties of Mycelium Composite Boards made from Lentinus sajor-caju with Various Ratios of Corn Husk and Sawdust. JoF 2024;10:634. https://doi.org/10.3390/jof10090634.

[53] Walter N, Gürsoy B. A Study on the Sound Absorption Properties of Mycelium-based Composites Cultivated on Waste Paper-based Substrates. Biomimetics 2022;7:100. https://doi.org/10.3390/biomimetics7030100.

[54] De G, Yang L, Lee J, Wu Y-H, Tian Z, Qin Z. Mycelium–coir-based composites for sustainable building insulation. J Mater Chem A 2025;13:9694–707. https://doi.org/10.1039/D4TA07869A.